New & Renewable Energy 2025. 12 Vol. 21, No. 4
ISSN 1738-3935 (Print)
ISSN 2713-9999 (Online)
https://doi.org/10.7849/ksnre.2025.0036
[2025-12-IES-006]

Check for updates

전기 · 수소 · 담수 동시 생산을 위한원자력–재생 하이브리드 에너지 시스템 모델링 및 시뮬레이션

Zuzhi Li[1] · 한승수[2] · 김형대[3]*

Modeling and Simulation of Nuclear Renewable Hybrid Energy Systems for Co-Production of Electricity, Hydrogen, and Clean Water

Zuzhi Li[1] · Seungsu Han[2] · Hyungdae Kim[3]*

Received 3 October 2025 **Revised** 15 December 2025 **Accepted** 15 December 2025 **Published online** 23 December 2025

ABSTRACT Nuclear renewable hybrid energy systems (NR-HESs) for multi-purpose applications are gaining increasing attention from the international nuclear energy community as well as energy system designers and policymakers—particularly in the context of deep decarbonization and net-zero targets. Over the past few decades, various modeling tools, such as mathematical formulations and Modelica, have been applied for analyzing the performance of NR-HESs; however, validating such results has been challenging due to the absence of a parallel simulation environment. In this study, Flownex—a high-fidelity 1D system simulation tool—was employed to enhance the verification and validation of NR-HES performance. A solar—nuclear combined centralized heating system was modeled using Flownex, showing improved electricity production (about 34%) and mitigation of the duck curve. Furthermore, a thermal and electricity (T&E) coupling strategy is implemented to integrate electrolyzers and reverse osmosis units for hydrogen and clean water production. Results indicated that hydrogen output increased by 31.80%, whereas clean water production improved by only 7.72%. The difference in coupling effectiveness is attributed to the higher sensitivity of hydrogen production to thermal energy.

Key words Nuclear renewable hybrid Energy system(원자력-재생 하이브리드 에너지 시스템), Centralized heating system(중앙집중식 난방 시스템), Thermal & electricity coupling(열-전력 커플링)

Nomenclature

N : total number solar collector

$\dot{q_s''}(t)$: solar heat flux, W/m^2

A_s : area of single solar collector panels, m^2

W_{net} : net power output of RC, KW

W_T : power of Turbine, KW

W_{RC} : power consumption of pump in RC, KW

Q_{RC} : Input heat of the RC, KW

η : efficiency of RC, %

η_{RC} : efficiency of pump in RC, %

ρ_l : density of water, Kg/m^3

Q_R : thermal power of reactor, MW

Q_S : thermal power of solar collector, MW

1) Master Candidate, Department of Nuclear Engineering, Kyung Hee University
2) Ph.D. Candidate, Department of Nuclear Engineering, Kyung Hee University
3) Professor, Department of Nuclear Engineering, Kyung Hee University
***Corresponding author:** hdkims@khu.ac.kr
Tel: +82-31-201-3322

T_i : temperature of node, °C
i : number of node.
$\dot{m}_R$: mass flow rate of reactor pump, Kg/s
$\dot{m}_{CHS}$: mass flow rate of pump in CHS, Kg/s
p_i : pressure of node, MPa
h_i : enthalpy of node, KJ/Kg
Q_{HEi} : heat transfer of heat exchanger, KW
W_{CHS} : power consumption of CHS pump, KW
Q_C : dispassion heat of condenser, KW
Q_{HTE} : thermal energy allocated for HTE, KW
γ_l : split ratio of net power of RC for electrolyzer, %
$Q_{loss,l}$: thermal loss of the electrolyzer, KW
T_l : water splitting efficiency of electrolyzer, %
l : HTE or LTE
W_{H_2} : power consumption for hydrogen production, KW
M_{H_2} : molar mass of hydrogen, g/mol
M_{H_2O} : molar mass of water, g/mol
$\dot{m}_{H_2}$: hydrogen production rate, g/s
ΔH_l : reaction enthalpy of water splitting, KJ/mol
$\dot{m}_{c,L}$: mass flow rate of cooling pump in LTE, Kg/s
$W_{c,H}$: power consumption of cooling water pump in LTE, KW
α : steam utilization efficiency, %
Q_{Ri} : heat transfer for thermal recover system, KW
$\dot{m}_{f,H}$: mass flow rate of feed water pump in HTE, Kg/s
$W_{f,H}$: power consumption of feed water pump in HTE, KW
$\dot{m}_{c,H}$: mass flow rate of circulation pump in HTE, Kg/s
$W_{c,H}$: power consumption of circulation water pump in HTE, KW
$Q_{R,HTE}$: total recovered heat for HTE, KW
$\dot{m}_g$: mass flow rate of specific components, Kg/s
Δh : the enthalpy changes of components, KJ/Kg
g : components which include HTE, HST_H, OCT
$\dot{m}_{f.L.1}$: the first source mass flow rate of feed water pump, Kg/s
p_{H_2O} : partial pressure of water vapor, KPa
$p_{sat}(T)$: the saturated vaper pressure at a given temperature, KPa
p_{LTE} : the total pressure of LTE, KPa.
p_m : the partial pressure of specific gas, KPa
R_m : the ideal gas constant of specific gas, J/(molK)
n_m : molar number of specific gasses, mol
$n_{H_2O,m}$: molar number of water power mixed with specific gas, mol
m : hydrogen or oxygen
$\dot{m}_{f.L.1}$: the second source mass flow rate of feed water pump, Kg/s
g : components which include OST_L, HST_L, LTE
Q_W : thermal energy allocated for WWRO from CHS, KW
$Q_{tot,W}$: total thermal energy that consumed by WWRO, KW
γ_n : split ratio of net power of RC for RO system, %
n : W for WWRO or C for CWRO
$\dot{m}_{h.n}$: the mass flow rate of high-pressure pump for different RO system, Kg/s
ρ_{sw} : density of seawater, Kg/m^3
Δp : pressure difference of inlet and outlet for high pressure pump, MPa.
η_p : efficiency of high-pressure pump, %
$R(T)$: the recovery rate of RO system, %
$\dot{m}_{RO1}$: the clean water production rate of first stage of RO system, Kg/s
$\dot{m}_{c,l}$: the mass flow rate of circulation pump for RO system, Kg/s
$\dot{m}_{tot}$: total mass flow rate of clean water, Kg/s
$Q_{R.W}$: the total recovery heat in WWRO, KW
T_O : the operation temperature of membrane in RO, K
p_O : the operation pressure of membrane in RO, MPa
F_p : the permeate flow rate of membrane in RO, m^3/d
t : represents the BT and CWT

b : represents the HT and CT
η_s : the efficiency of PV system, %
N' : number of solar collectors for duck curve mitigation
x : HTE for high temperature electrolyzer, W for WWRO
R : the ratio that indicate the fraction of thermal energy for rising system temperature, %
Q_E : electricity equivalent thermal energy, KW

Subscript

NR-HES : nuclear renewable hybrid energy system
SC : solar collector
RC : Rankine cycle
DCs : duck curves
T&E : thermal and electricity
S&N : Solar and nuclear energy
ALE : alkaline liquid electrolysis
PVS : photovoltaic system
SOE : solid oxide electrolysis
CHS : centralized heating system
SMMSR : small modular molten salt reactor
HTE : high temperature electrolyzer
LTE : low temperature electrolyzer
OCT : oxygen storage tank
BT : brine tank
CWT : clean water tank
HST_H : high temperature hydrogen separation tank
OST_L : low temperature oxygen separation tank
HST_L : low temperature hydrogen separation tank
WWRO : warm water reverse osmosis

1. Introduction

In general, the two principal options for low-carbon energy are renewable and nuclear energy. The potential synergies between them, as well as the advantages of their integration, have not yet been fully explored. NR-HES combine these generation sources to leverage the strengths of each technology, thereby providing reliable and sustainable electricity to the grid while also supplying low-carbon energy to other sectors. Such systems can produce heat, electricity, and other essential products, while supporting higher penetrations of variable renewable generation.[1]

NR-HES are typically defined as integrated facilities comprising nuclear reactors, renewable energy generation, and industrial processes that simultaneously address grid flexibility, greenhouse gas (GHG) emission reduction, and efficient use of investment capital. These systems are often described as integrated energy systems that incorporate multiple generators and deliver multiple energy products, either as coordinated systems or tightly coupled energy systems.[2,3]

Over the past few years, many research groups have studied the system integration and different coupling strategies to optimize the performance of NR-HES. In 2023, a multi-objective optimized multi-energy complementary integrated energy systems has been proposed, with the consideration of load prediction and renewable energy production uncertainties. The proposed multi-energy complementary distributed energy system presents an economic benefit (reducing 25% of the annual total cost) compared to a gas turbine-based integrated energy system.[4] Furthermore, a recently published study analyzed integration of green hydrogen production with renewable energy-power desalination.[5] This work is innovative as it not only links these two supply systems to enhance the integration of intermittent renewable energy but also conducts an extensive economic analysis of combining two different renewable energy sources. Additionally, a multi-energy complementary energy system has been proposed to integrate waste heat and surplus electricity for hydrogen production, indicating the hydrogen production's profit rate is approximately 70%.[6] Another literature analyzed the pumped thermal energy storage system combined cold, heat, and power generation. The designed system can achieve a total energy efficiency of 2.39 and a

high thermal economic performance.[7] More recently, through the multi-objective evolutionary algorithms, Ji *et al.* optimize the nuclear solar hybrid energy systems (NSHES) that simultaneously considers both cost and power supply stability. The optimized NSHES offers an effective approach to mitigating the mismatch between energy supply and demand.[8] However, previous research conducted system integration and different coupling strategies to optimize the performance NR-HES by mathematical modeling, which is challenging to present the detail system configuration and their thermohydraulic property, thereby deter the realistic implementation of these optimization strategies.

Except the mathematical modeling, the precise 1D simulation environment such Modelica has been widely used to investigate the performance of NR-HES. The Oak Ridge National Laboratory (ORNL) developed the physical model for different configuration of NR-HES including the primary heating system, thermal energy storage system, hydrogen electrolyzer and dynamic controlling system, etc.[9,10] Wang *et al.* compared the performance of reverse osmosis and freeze desalination (FD) in producing the clear water by NR-HES. They found that the FD system was able to boost the power production by about 12% by making the steam cycle over 2% more efficient.[11] More recently, Masotti *et al.* extended the use of components in NR-HES for the analysis and simulation of various architectures. This research indicated that the overall efficiency significantly improved in NHES incorporating TES and using nuclear heat to drive non-electric applications.[12] Furthermore, based on the open source provided by ORNL, Zhang *et al.*, developed the dynamic control of the integrated energy system and its components with the consideration of various demand and atmospheric conditions.[13] However, the previous study only used the Modelica to conduct the simulation, it is hard to validate the accuracy of simulation results. Additionally, there are very limited number of papers focusing on the multiple objective optimizations, thereby limited the robustness of simulation results.

Therefore, coupling with non-electric applications involving the use of heat and production of commodities, such as hydrogen or potable water, would require further developments and adaptation for existing technologies, which relies on considerable testing and validation, modelling and advanced simulation tool. In addition, the wide variety of subcomponents and interconnections needed to be managed in real time, and in an efficient manner, as well as deep understanding of the system architecture that will have case specific features and characteristics.[3]

The Flownex SE simulation can provide the realistic and dynamic behavior of nuclear renewable hybrid energy system.[14] It can be served as second party to completely validate the simulation results. By extracting the detail hydraulics properties of components, including pipe dimeter, length, it can provide the valuable insights to assist the real construction of nuclear renewable hybrid energy system. Also, based on the predicted results given by Flownex, it can avoid potential accidents such as most probable pipe corrosion or break according to the maximum velocity prediction. As a first try of using Flownex to simulate the NR-HES, the primary objective of this study is to investigate how the performance of NR-HES can be improved through the CHS and T&E coupling.

As illustrated in Fig. 1, the solar collector, integrated with the nuclear reactor, stores thermal energy in the CHS, which consists of a hot storage tank and a cold storage tank. The stored thermal energy can be utilized in two ways. First, the CHS directly supplies thermal energy to the HTE and WWRO systems to raise their operating temperatures. Second, through a heat exchanger connecting the CHS to the Rankine cycle (RC), thermal energy is converted to electricity by the turbine, which then powers the different subsystems. To further improve the efficiency of the integrated system and enhance hydrogen and clean water production, a waste heat recovery system is also

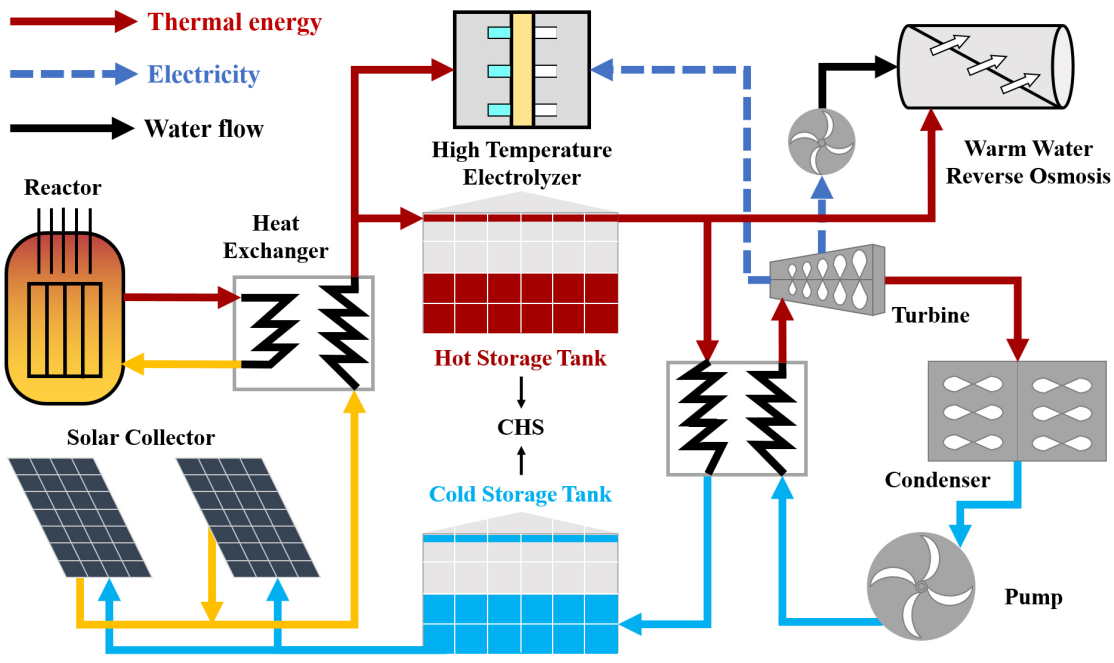

Fig. 1. Conceptual nuclear–renewable HES with T&E coupling and CHS for RO and THE

incorporated. To reveal the effectiveness of above coupling strategy, the traditional systems are selected to be compared.

The total production of traditional system including the electricity, water and hydrogen mass flow rate is calculated as summation of individual power source including the nuclear power and PV solar system.

Furthermore, the traditional system does not incorporate T&E coupling; instead, it supplies electricity only, which is used by the LTE and CWRO systems to produce hydrogen and clean water. Based on the above comparison, the research objectives of this study can be further divided into two specific aspects:

(1) To evaluate the ability of CHS in enhancing the electricity generation while mitigating DCs.

(2) To assess the effectiveness of the T&E coupling strategy in enhancing clean water and hydrogen production, while revealing the main factor in influencing the performance of T&E coupling strategy.

Flownex, a one–dimensional (1D) thermo–fluid simulation software, is used to realistically investigate the advantages of CHS and effectiveness of T&E in improving water and hydrogen production by suitably allocating the thermal energy distribution in different subsystems.

2. System Description

In this section, the detailed assumptions for CHS, clean water and hydrogen production are introduced individually.

2.1 Centralized Heating System (CHS)

As shown in Fig. 2, nuclear and solar energy are combined to supply thermal energy for the CHS. Table 1 lists the main design parameters of the CHS. For the solar collector, the total number of panels is set to 150,000, each with a width of 1 m and a length of 2 m.[15] To simplify the problem, the total simulation period is assumed to be one week, with identical daily weather conditions (solar heat flux). The daily average solar heat flux of Jeju Island during March is used for

Table 1. The main design parameters of CHS

Parameters	Symbol	Range (Value)	Unit
Reactor thermal power	Q_R	120	MW
Solar thermal power	Q_S	0 - 227	MW
Reactor inlet temperature	T_1	438-603	℃
Reactor outlet temperature	T_2	536-702	℃
Temperature of HT	T_5	494-580	℃
Temperature of CT	T_8	325-340	℃
Mass flow rate of reactor pump	$\dot{m}_R$	600	kg/s
Mass flow rate of pump in CHS	$\dot{m}_{CHS}$	600	kg/s
Turbine inlet temperature	T_{26}	314 - 353	
Turbine inlet pressure	p_{26}	10.3-13.5	MPa

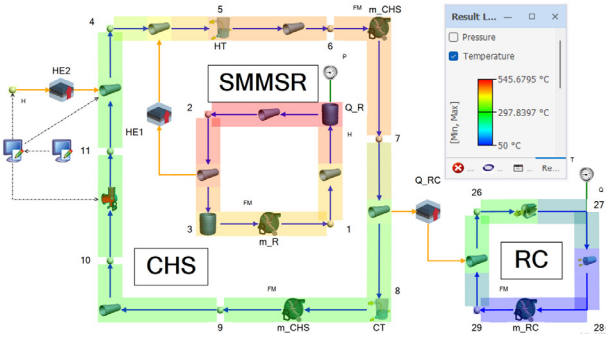

Fig. 2. The temperature contour of CHS

the simulation.[16] The thermal energy from the SC can be simply calculated as:

$$Q_{SC} = N \cdot \dot{q_s''}(t) \cdot A_s [MW] \quad (1)$$

Given the significant diurnal variation in solar heat flux, temperatures throughout the system (notably in the CHS and SMMSR) vary over time. Therefore, key design parameters are presented as ranges instead of single fixed values to reflect these operating conditions. For the nuclear system, a SMMSR with a constant thermal power of 120 MW is selected as the nuclear energy source.[17] As shown in Fig. 2, both the SMMSR and solar collectors supply thermal energy to the CHS, which (i) delivers heat input to the Rankine cycle and (ii) heats the molten salt in the hot tank (HT) and cold tank (CT). The operating pressure of the SMR and CHS is set to 500 kPa.[18] The outlet and inlet temperatures of the SMMSR are assumed to fall within 536~702℃ and 438~603℃, respectively.[19] For the CHS, the HT and CT temperatures are maintained within 494~580℃ and 325~340℃, respectively.[20] The maximum system pressure, which occurs at the turbine inlet of the Rankine cycle, is designed to range from 10.3 to 13.5 MPa.[20] The turbine inlet temperature is set between 314~353℃, while the outlet temperature is fixed at 50℃.[20] To account for system pressure losses, all piping is assigned a surface roughness of 45 μm.[21] To be clear, h_{29} and h_{28} represent the pump outlet and inlet enthalpy, respectively.

For an incompressible liquid, the pump outlet enthalpy was calculated using the standard relation:

$$h_{29} = h_{28} + \frac{p_{29} - p_{28}}{\rho_l \cdot \eta_{RC}} [KJ/Kg] \quad (2)$$

This assumption is commonly applied for liquid pumps because the temperature change is negligible and the fluid is treated as incompressible. We also conduct an energy analysis to establish a thermo-dynamic model for evaluating the performance of the CHS. To simplify the modeling process, heat losses from the heat exchangers to the external environ-ment are neglected, except for the condenser, which primarily functions as a heat rejection unit. The energy conservation equations for the main components of both systems are derived from the first law of thermody-namics and are summarized in Table 2. The net power output of the Rankine cycle (RC) is calculated as:

$$W_{net} = W_T - W_{RC} [MW] \quad (3)$$

The cycle efficiency is defined as the ratio of the net output work to the input heat. It can be expressed as:

Table 2. The energy conservation equation of main components in CHS

Components	Energy conservation equation
SMMSR	$Q_R = \dot{m}_R \cdot (h_2 - h_1)$
Reactor pump	$W_R = \dot{m}_R \cdot (h_1 - h_3)$
Heat exchanger 1	$Q_{HE1} = \dot{m}_R \cdot (h_2 - h_3) = \dot{m}_{CHS} \cdot (h_5 - h_6)$
Heat exchanger 2	$Q_{HE2} = \dot{m}_R \cdot (h_2 - h_3) = N \cdot q_s''(t) \cdot A_{tat}$
CHS pump	$W_{CHS} = \dot{m}_{CHS} \cdot (h_7 - h_6 + h_2 - h_9)$
Heat exchanger RC	$Q_{RC} = \dot{m}_{RC} \cdot (h_{26} - h_{29}) = \dot{m}_{CHS} \cdot (h_7 - h_8)$
Turbine	$W_T = \dot{m}_{RC} \cdot (h_{26} - h_{27})$
RC pump	$W_{RC} = \dot{m}_{RC} \cdot (h_{29} - h_{28})$
Condenser	$Q_C = \dot{m}_{RC} \cdot (h_{27} - h_{28})$

$$\eta = \frac{W_{net}}{Q_{RC}} [\%] \tag{4}$$

The net output power is partially allocated to the hydrogen electrolyzer and reverse osmosis system, enabling the production of hydrogen and clean water.

2.2 Hydrogen Production

2.2.1 Assumptions

For hydrogen production, two different types of electrolyzer are considered to verify the effectiveness of the T&E coupling strategy. As shown in Fig. 5, unlike the LTE, which is powered solely by electricity, the HTE first receives thermal energy (Q_{HTE}) from the CHS to heat water into high–temperature vapor, while a portion of the turbine's net power is simultaneously supplied to the electrolyzer. Accordingly, the total thermal energy consumption of the HTE can be expressed as:

$$Q_{tot,HTE} = Q_{HTE} + \gamma_{HTE} \cdot Q_{RC} [KW] \tag{5}$$

where the $\gamma_{HTE} \equiv 0.01$. To enable a fair comparison of hydrogen production, the portion of electricity supplied to the LTE is adjusted to a higher value such that the total thermal energy consumption matches that of the HTE. The split ratio of the net turbine power allocated to the LTE can therefore be calculated as:

$$\gamma_{LTE} = \frac{Q_{HTE} + \gamma_{HTE} \cdot Q_{RC}}{Q_{RC}} = \gamma_{HTE} + \frac{Q_{HTE}}{Q_{RC}} [\%] \tag{6}$$

During the water–splitting reaction in the electrolyzer, the supplied electricity is divided into two contributions. One portion drives the electrochemical reaction, producing hydrogen and oxygen, while the remaining portion is dissipated as heat through ohmic losses and auxiliary components. This dissipated fraction raises the system temperature and is defined in this study as the thermal loss of the electrolyzer (Q_{loss}).

$$Q_{loss,l} = W_{net} \cdot \gamma_l \cdot (1 - \varepsilon_l) [KW] \tag{7}$$

Considering that the Faradaic efficiency of the hydrogen electrolyzer is approximately unity,[22] it is assumed that all electrochemical products are hydrogen. The electricity used for hydrogen production can be expressed as:

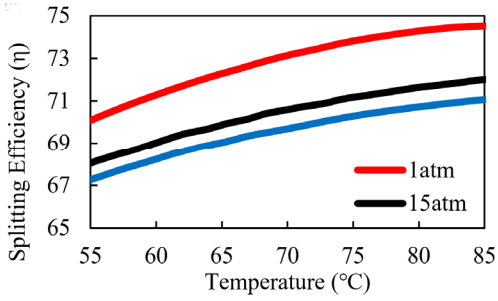

Fig. 3. The water splitting efficiency of LTE at different pressure[19]

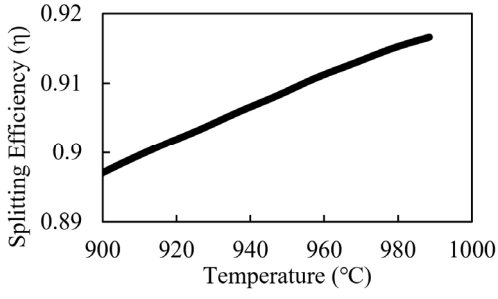

Fig. 4. Theoretical Thermal water splitting efficiencies of HTE at 500 KPa[20]

$$W_{H_2} = W_{net} \cdot \gamma_l \cdot \varepsilon_l \; [KW] \tag{8}$$

The hydrogen production rate can be calculated as:

$$\dot{m}_{H_2} = \frac{W_{H_2}}{\Delta H_l} \cdot M_{H_2} \; [Kg/s] \tag{9}$$

To determine the water-splitting efficiency, a further literature survey was conducted. As shown in Figs. 3 and 4, for both LTE and HTE, higher system temperatures within a suitable range correspond to higher splitting efficiencies.[23,24]

In this study, to simplify the analysis, we assume a linear correlation between electrolysis temperature and splitting efficiency. To ensure the validity of this assumption, the operating temperatures of the HTE and LTE are maintained within 947~975℃ and 55~85℃, respectively. As shown in Fig. 5, the LTE is operated at 1 atm to optimize hydrogen production, while the HTE operates at 500 kPa.[24] Table 3 summarizes the main design parameters of the HTE and LTE. The energy conservation equations for the main components of both systems are derived from the first law of thermodynamics and are presented in Table 4.

Table 3. The main parameters of HTE and LTE

Parameters	Symbol	Range (Value)	Unit
Temperature of HTE	T_{HTE}	947–975	℃
Pressure of HTE	p_{HTE}	500	KPa
Temperature of LTE	T_{LTE}	60–80	℃
Pressure of LTE	p_{LTE}	101	KPa
LTE cooling pump	$\dot{m}_{c,L}$	0.6	kg/s
Steam utilization efficiency	α	85	%

Table 4. The energy conservation equation of main components in HTE and LTE

Component	Energy conservation equation
Recovered Heat 1	$Q_{R1} = \dot{m}_{O_2,H} \cdot (h_{16} - h_{17}) = \dot{m}_{f.H} \cdot (h_{15} - h_{14})$
Recovered Heat 2	$Q_{R2} = \dot{m}_{c,H} \cdot (h_{19} - h_{20}) = \dot{m}_{f.H} \cdot (h_{16} - h_{15})$
Recovered Heat 3	$Q_{R3} = \dot{m}_{H_2,H} \cdot (h_{22} - h_{21}) = \dot{m}_{c.H} \cdot (h_{23} - h_{24})$
Heat input of HTE	$Q_{HTE} = \dot{m}_{CHS,H} \cdot (h_6 - h_5) = \dot{m}_{c.H} \cdot (h_{14} - h_{13})$
HTE feed water pump	$W_{f,H} = \dot{m}_{f.H} \cdot (h_{13} - h_{12})$
THE circulation pump	$W_{c,H} = \dot{m}_{c.H} \cdot (h_{24} - h_{25})$
LTE cooling pump	$W_{c,L} = \dot{m}_{c.H} \cdot (h_{24} - h_{25})$
LTE feed water pump	$W_{f,L} = \dot{m}_{f.L} \cdot (h_{44} - h_{50})$

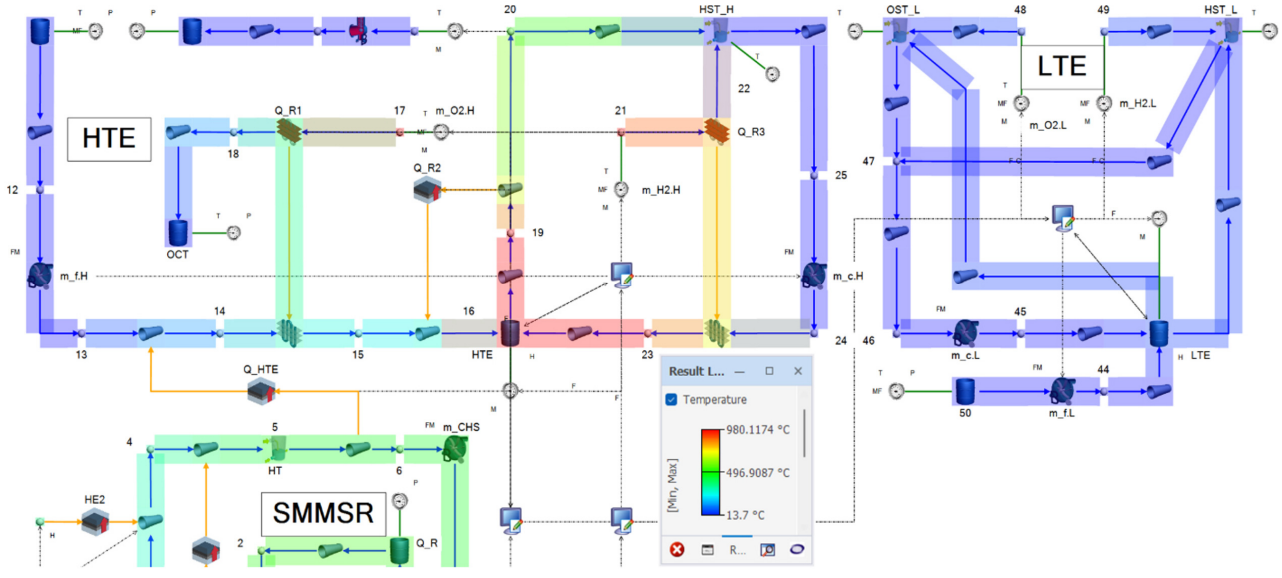

Fig. 5. The temperature contour of HTE and LTE

2.2.2 Specific Design of THE

For the HTE, the total water supply consists of two sources: (i) the mass flow rate from the feed water pump, which is determined based on the transient requirements of the electrolyzer and can be expressed as:

$$\dot{m}_{f.H} = \dot{m}_{H_2} \cdot \frac{M_{H_2O}}{M_{H_2}} \; [Kg/s] \tag{10}$$

(ii) Considering the steam utilization efficiency in the HTE, the actual input water mass is greater than the electrolysis consumption. To compensate for this additional water requirement, a circulation pump is incorporated into the HTE, with its mass flow rate expressed as follows:

$$\dot{m}_{c.H} = \dot{m}_{f.H} \cdot \left(\frac{1}{\alpha} - 1 \right) \; [Kg/s] \tag{11}$$

The total recovered heat for the HTE can then be expressed as:

$$Q_{R,HTE} = Q_{R1} + Q_{R2} + Q_{R3} \; [KW] \tag{12}$$

The energy conservation equation for the HTE can be expressed as:

$$\begin{aligned} &Q_{HTE} + W_{f,H} + W_{c,H} + W_{net} \cdot \gamma_{HTE} \\ &= W_{H_2} + \sum_g \dot{m}_g \cdot \Delta h \; [KW] \end{aligned} \tag{13}$$

2.2.3 Specific Design of LTE

Unlike the HTE, the feed water for the LTE must satisfy requirements from two sources: (i) the water consumed by the electrochemical reaction, and (ii) the mixed vapor flow of hydrogen and oxygen. The mass flow rate for the first source can be calculated using the following equation:

$$\dot{m}_{f.L.1} = \dot{m}_{H_2} \cdot \frac{H_{H_2O}}{M_{H_2}} \; [Kg/s] \tag{14}$$

To determine the mass flow rate of water in the mixed hydrogen–oxygen flow, we first assume that the partial pressure of water vapor is equal to the saturation vapor pressure at the given temperature T.[25]

$$p_{H_2O} = p_{sat}(T) \; [KPa] \tag{15}$$

Considering that oxygen and hydrogen are produced separately at the anode and cathode, the pressure within the electrolyzer is assumed to be the same in both chambers. Therefore, the total pressure of the water vapor mixed with oxygen and hydrogen can be expressed as:

$$p_{LTE} = p_{H_2O} + p_{H_2} = p_{H_2O} + p_{O_2} \; [KPa] \tag{16}$$

According to the ideal gas law, the mole fraction of water vapor in the mixture with oxygen and hydrogen can be expressed as:

$$\frac{n_{H_2O,m}}{n_m} = \frac{R_m p_{H_2O}}{R_{H_2O} p_m} \; [\%] \tag{17}$$

where R is the ideal gas constant, and the subscript m refers to hydrogen in the cathode chamber or oxygen in the anode chamber. The second mass flow rate can then be expressed as:

$$\dot{m}_{f.L.2} = \sum_m n_{H_2O,m} \cdot M_{H_2O} \; [Kg/s] \tag{18}$$

The total feed water mas flow rate can be given as:

$$\dot{m}_{f.L} = \dot{m}_{f.L.2} + \dot{m}_{f.L.1} \; [Kg/s] \tag{19}$$

The energy balance of LTE can be expressed as:

$$W_{c,L} + W_{f,L} + W_{net} \cdot \gamma_{LTE} = W_{H_2} + \sum_k \dot{m}_k \cdot \Delta h \ [KW] \quad (20)$$

2.3 Clean Water Production

In this study, a reverse osmosis (RO) system is selected for clean water production. As shown in Fig. 6, to evaluate the effectiveness of the T&E coupling strategy, both the WWRO and CWRO systems are considered for comparison of clean water production rates. Similar to the hydrogen production system, a portion of electricity is supplied to the high-pressure pump to maintain the required operating pressure of the RO system. The RO system consists of two membranes, denoted as RO_1 and RO_2. Compared with the CWRO, the WWRO additionally receives thermal energy from the CHS (Q_W). Therefore, the total thermal energy consumption of the WWRO can be expressed as:

$$Q_{tot,W} = Q_W + \gamma_W \cdot Q_{RC} \ [KW] \quad (21)$$

where ($\gamma_W = 0.01$). To more fairly compare the hydrogen production, a portion of electricity to higher pressure pump in CWRO is adjusted to a higher value to ensure same total thermal energy consumption. Therefore, the split ratio of net turbine power to CWRO high pressure pump can be calculated as:

$$\gamma_C = \frac{Q_W + \gamma_W \cdot Q_{RC}}{Q_{RC}} = \gamma_W + \frac{Q_W}{Q_{RC}} \ [\%] \quad (22)$$

The mass flow rate of high-pressure pump can be expressed as:

$$\dot{m}_{h.n} = \frac{\gamma_n \cdot W_{net} \cdot \rho_{sw}}{\Delta p} \cdot \eta_p \ [Kg/s] \quad (23)$$

For the first stage of membrane, the clean water production rate can be expressed as:

$$\dot{m}_{RO1} = \dot{m}_{h.n} \cdot R(T) \ [Kg/s] \quad (24)$$

After the first-stage membrane, the circulation pump supplies the remaining water mass flow rate to the

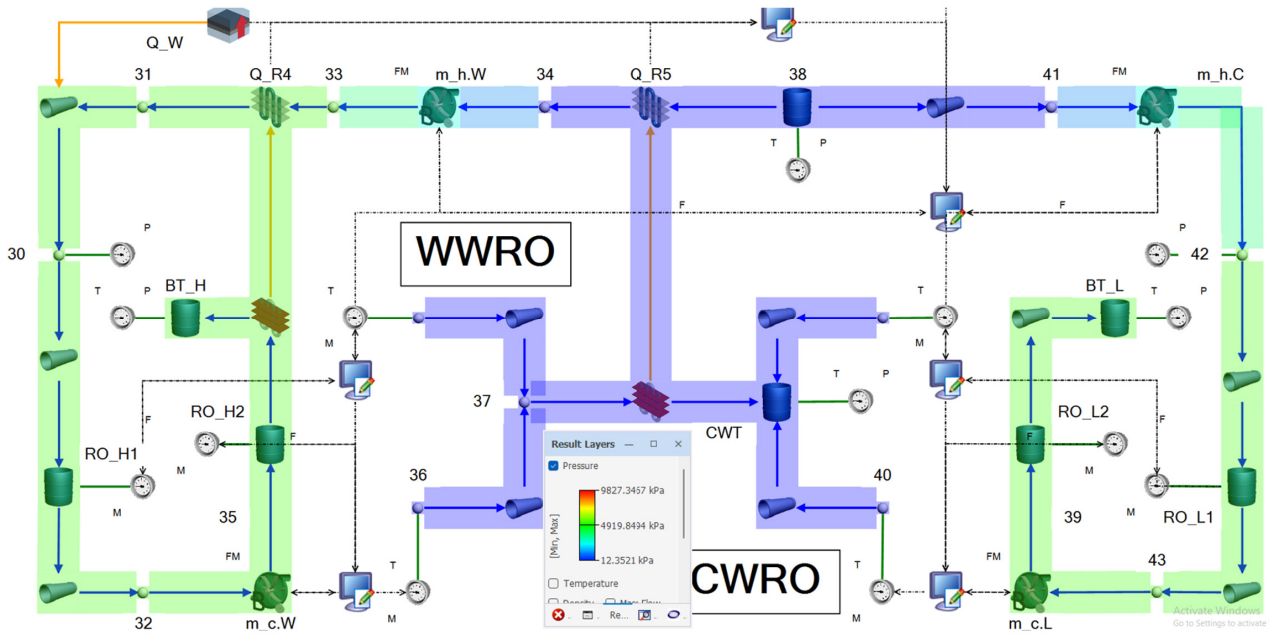

Fig. 6. The pressure contour of WWRO and CWRO

second-stage membrane. The mass flow rate of the circulation pump can be expressed as:

$$\dot{m}_{c,n} = \dot{m}_{h.n} \cdot (1 - R(T)) \ [Kg/s] \quad (25)$$

Therefore, the total clean water production can be calculated as:

$$\dot{m}_{tot} = \dot{m}_{c,n} \cdot R(T) + \dot{m}_{h.n} \cdot R(T) \ [Kg/s] \quad (26)$$

To clarify the effect of temperature on the performance of the RO system, a further literature survey was conducted. As shown in Fig. 7, within the operating temperature range of 20°C to 36°C, each 1°C increase results in approximately a 3% increase in the permeate flow rate of the reverse osmosis system.[26] To more precisely determine the correlation between system temperature and the recovery rate of a single membrane, the SWC5-LD membrane from Xylem Inc. was selected as a reference.[27] As shown in Table 5, at 25°C and 5.5 MPa, the permeate flow rate is 34.1 m^3/d with a recovery rate of 10%. For simplicity, it is assumed that the recovery rate of the membrane varies linearly with system temperature. Table 6 summarizes the main design parameters of the WWRO and CWRO systems. The total recovered heat for WWRO can be expressed as:

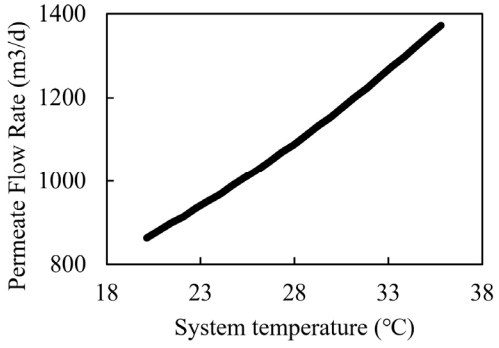

Fig. 7. The effect of temperature on permeates flow rate[22]

Table 5. The parameters of membrane SWC5-LD[23]

Parameters	Symbol	Value	Unit
Operating temperature	T_O	25	℃
Permeate flow rate	F_p	34.1	m^3/d
Operating pressure	p_O	5.5	MPa
Recovery rate	$R(T)$	10	%

$$Q_{R.W} = Q_{R4} + Q_{R5} \ [KW] \quad (27)$$

The energy balance of the main components is summarized in Table 7. Based on the above configuration and energy balance, the energy conservation equation for the WWRO can be expressed as:

$$Q_W + \gamma_W \cdot W_{net} + W_{c,W} = W_{h,W} + \sum_t \dot{m}_t \cdot \Delta h \ [KW] \quad (28)$$

Similarly, the energy conservation equation for CWRO can be expressed as:

$$\gamma_C \cdot W_{net} + W_{c,C} = W_{h,C} + \sum_t \dot{m}_t \cdot \Delta h \ [KW] \quad (29)$$

Table 6. The main parameters of WWRO and CWRO

Parameters	Symbol	Value (range)	Unit
WWRO temperature	T_W	31.8-31.2	℃
WWRO pressure	P_W	5.5	MPa
CWRO temperature	T_W	14.26	℃
CWRO pressure	P_C	5.5	MPa
Recovery rate of WWRO	R_W	6.8	%
Recovery rate of CWRO	R_C	11.8-12	%

Table 7. The energy conservation equation of main components in WWRO and CWRO

Component	Energy conservation equation
Recovered Heat 5	$Q_{R5} = \dot{m}_{h,W} \cdot (h_{34} - h_{38})$
Heat input of WWRO	$Q_{R3} = \dot{m}_{h,W} \cdot (h_{30} - h_{31})$
WWRO high pressure pump	$W_{h,W} = \dot{m}_{h,W} \cdot (h_{33} - h_{34})$
WWRO circulation pump	$W_{c,W} = \dot{m}_{c,W} \cdot (h_{35} - h_{32})$
CWRO high pressure pump	$W_{h,C} = \dot{m}_{h,C} \cdot (h_{42} - h_{41})$
CWRO circulation pump	$W_{c,C} = \dot{m}_{h,C} \cdot (h_{39} - h_{43})$

3. System integration

In this section, the overall integrated system is shown in Fig. 8. The system is designed to simultaneously produce hydrogen and clean water. On one hand, the CHS directly supplies thermal energy to various sub-systems, such as the electrolyzer and reverse osmosis system; on the other hand, thermal energy is fed into the Rankine cycle (RC) to generate electricity. Based on the Flownex diagram and the energy balance of each component described in the previous sections, the energy conservation equation for the CHS can be

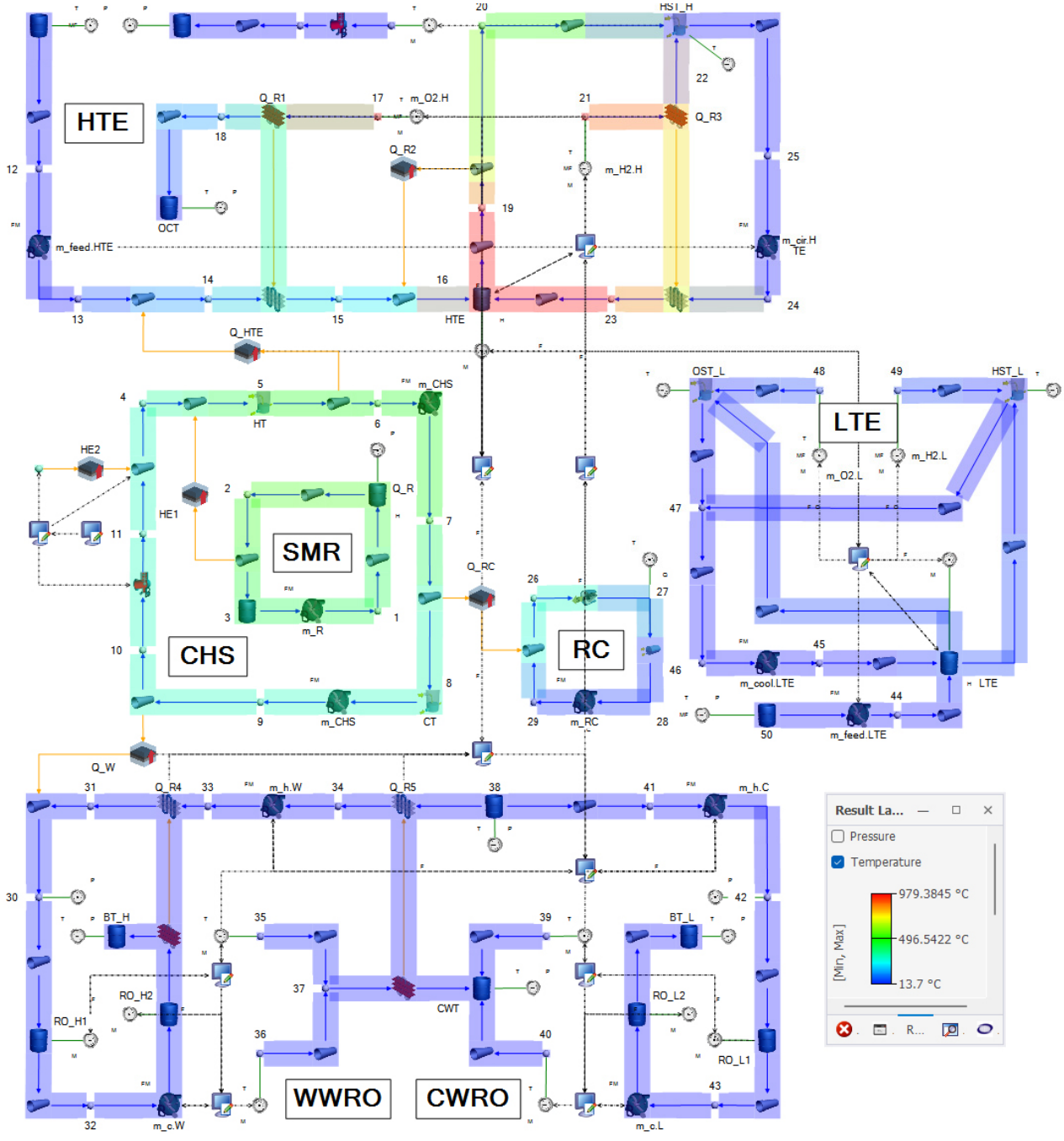

Fig. 8. The temperature contour of Integrated system

expressed as:

$$W_{CHS}+Q_{HE1}+Q_{HE2}=Q_{RC}+Q_{HTE}+Q_W + \sum_t \Delta T \cdot c_p \cdot \dot{m}_t \ [KW] \quad (30)$$

The net power of the whole integrated system can be written as:

$$W_{NET}=W_T-W_R-W_{CHS}-W_{f,H}-W_{c,H}-W_{RC}- W_{f,L}-W_{c,L}-W_{h,W}-W_{c,W}-W_{h,L}-W_{c,L} \quad [KW] \quad (31)$$

4. Results and Discussions

The section is organized into two parts. First, the role of the CHS is examined in terms of its ability to mitigate the duck curve and enhance electricity production. Second, the impact of the T&E coupling strategy is analyzed, highlighting its potential to improve hydrogen and clean water production, which is strongly influenced by the system's sensitivity to thermal energy.

4.1 Effect of CHS

Fig. 9 shows the electricity production of the CHS over time. To evaluate the effectiveness of coupling solar and nuclear systems (S&N coupling) in enhancing electricity output, the electricity produced by the traditional system is calculated as the sum of the individual outputs from solar and nuclear sources. To fairly represent the effect of S&N coupling, electricity from each source is assumed to use the same CHS configuration. Consequently, the turbine power generated solely by solar energy is compared with that of the S&N coupling system. At the initial stage, the turbine power for the solar–only case is nearly zero, resulting in a large gap compared with the S&N coupling scenario. This initial gap is primarily due to the contribution of nuclear energy, with the turbine power from nuclear input estimated as $P_{ini} \approx 40.9\,MW$. For both cases, turbine power initially exhibits unstable fluctuations before transitioning to a stable oscillatory behavior However, the S&N coupling system reaches stability in only three days, compared with 6~7 days for the solar–only case. This behavior is attributed to the large total heat capacity of the CHS: during the early stage, the combined solar and nuclear inputs are insufficient to fully charge the CHS, resulting in unstable power output. As the system approaches equilibrium between heat input and output, stable and periodic fluctuations in electricity generation occur. To comprehensively evaluate turbine performance, the maximum power ($P_{\max}$), minimum power ($P_{\min}$) and average power (P_{avg}) during the stable state are selected for further analysis. As shown in Table 8, the power fluctuation (ΔP) is defined as the difference between $P_{\max}$ and $P_{\min}$, while the average power P_{avg} is calculated as the mean of

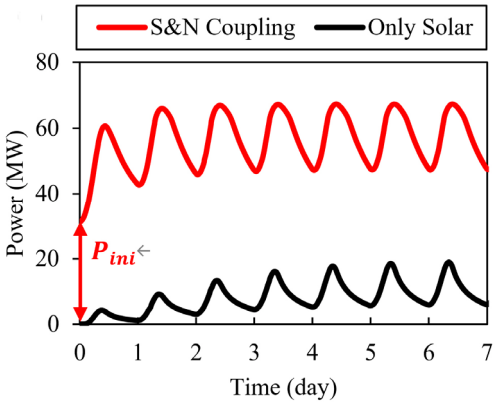

Fig. 9. The Power Production of CHS during a week

Table 8. Comparison of Electricity production between CHS and traditional system

Energy Source	$P_{\max}$	$P_{\min}$	P_{avg}	ΔP
Solar energy	19.19	5.97	12.58	13.22
Nuclear energy		31.13		0
Traditional system	50.32	37.1	43.71	13.22
S&N coupling	67.44	47.28	57.36	20.16
Enhancement	34%	27.4%	31.2%	52.7%

P_{max} and P_{min}. All power values are expressed in megawatts (MW). The results indicate that the S&N coupling not only achieves higher electricity production (approximately 31.2% improvement compared with the traditional system) but also reduces power fluctuations by 52.7%. The large power fluctuation can be attributed to shortage of energy controlling system. This aspect will be included in our future work.

To clearly illustrate the duck-curve mitigation effect of the CHS, the same solar heat flux is applied to two sets of solar collectors, each with the same number of panels and total area. In the first case, one set of solar collectors is connected to the CHS, where solar energy is first converted into thermal energy and subsequently transformed into electricity via the RC. In the second case, the other set of solar collectors is directly connected to a photovoltaic system (PVS), which converts solar energy directly into electricity without intermediate thermal storage. Therefore, the electricity produced by the PVS can be expressed as:

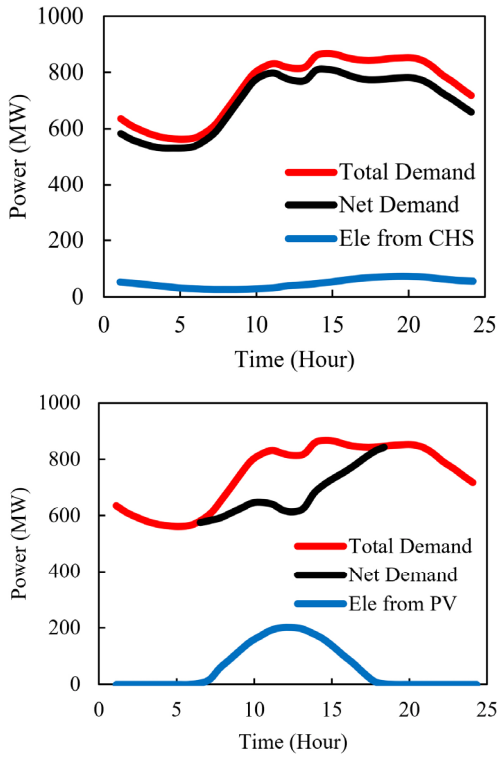

Fig. 10. DCs generated by CHS (up), PVS (down)

$$P_{PVS} = N' \cdot q_s'' \cdot A_{tot} \cdot \eta \ [MW] \quad (32)$$

It is worth noting that this value differs from the assumption given in the previous chapter. The purpose of using a larger value is to more clearly demonstrate the duck-curve mitigation effect provided by the CHS. Additionally, as shown in Fig. 10, the total power demand (red line) of Jeju Island during March 2024 is used to illustrate the duck curves (DCs).[28]

The two methods are expected to produce different DCs, which are compared to evaluate the effect of the CHS in mitigating the duck curve. Specifically, the electricity generated by the CHS is denoted as P_{CHS}, with its corresponding duck curve labeled as DC1, while the PVS-generated electricity is labeled DC2. The net demand is defined as the difference between the total demand and either P_{CHS} or P_{PVS}. For DC1, since solar energy is converted into thermal energy and stored in the CHS, the power output is more evenly distributed throughout the day rather than concentrated during daytime. Consequently, the resulting electricity profile is smoother compared with that of the PVS, and the net demand does not exhibit the typical duck-shaped pattern. In contrast, for the traditional PVS, electricity generation occurs only during daytime, creating a significant gap between total demand and net demand. Thus, the duck curve is clearly observed in the PVS case but is effectively mitigated by the CHS.

4.2 The Effect of T&E coupling

The hydrogen electrolyzer and water reverse osmosis system exhibit production curves similar to those of electricity generation. As shown in Fig. 11, the HTE achieves significantly higher hydrogen production compared with the LTE, with an improvement of approximately 31.8%. In contrast, the WWRO shows only a modest increase in clean water production, around 7.72%. These results indicate that the T&E coupling strategy exhibits varying levels of effectiveness

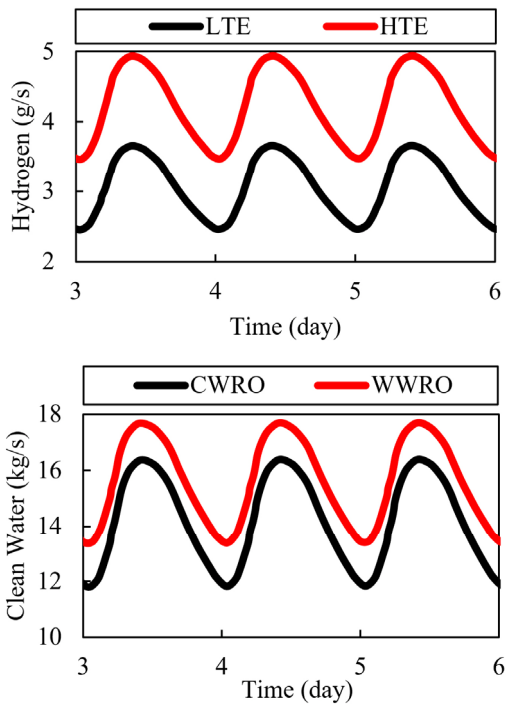

Fig. 11. The hydrogen (up) and clean water (down) production with and without T&E coupling

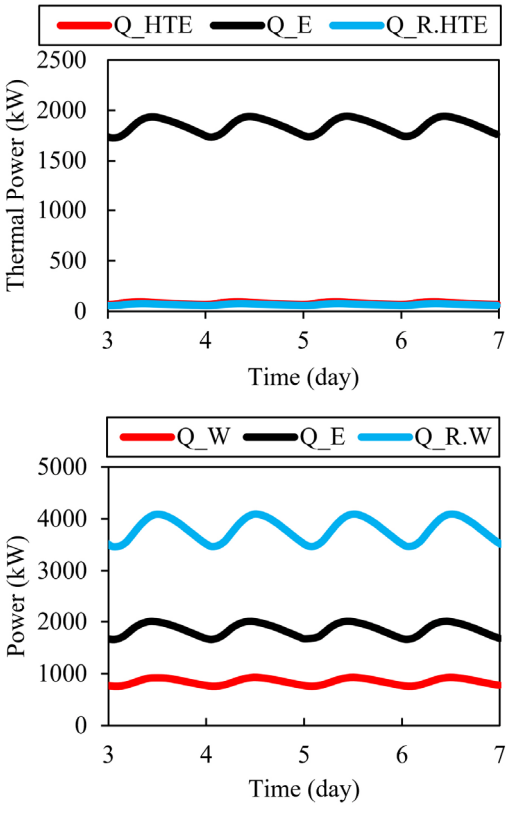

Fig. 12. The thermal energy distribution in HTE (up) and WWRO (down)

for different products. To further clarify the reasons for these differences in production, the thermal energy distribution was analyzed in detail. As shown in Fig. 12, the HTE and WWRO exhibit different thermal energy distributions.

To be clear, the electricity that induced to HTE and WWRO is converted into thermal energy to fairly compare with other thermal energy contribution. Therefore, the electricity equivalent thermal energy is written as:

$$Q_E = \frac{W_{net}}{\eta} \cdot \gamma = Q_{RC} \cdot \gamma \ [KW] \tag{33}$$

For hydrogen production, Q_E dominates, accounting for approximately 89% of the total thermal energy, while the combined contributions of $Q_{R.HTE}$, Q_{HTE} make up only about 11%. In contrast, for clean water production, a larger proportion of thermal energy Q_W about 17.73% is allocated to increasing the system temperature compared with HTE. Notably, the $Q_{R.W}$ accounts for a dominant 56%, indicating that the thermal energy recovery system is particularly critical for the WWRO.

To more clearly represent the thermal energy distribution among the different systems, a ratio (R) is defined as:

$$R = \frac{Q_x + Q_{R.x}}{Q_{R.x} + Q_E + Q_x} \ [\%] \tag{34}$$

where subscript x represents the HTE for the high temperature electrolyzer or W for WWRO. Physically, this ratio represents the proportion of the total thermal energy allocated to increasing the system temperature.

As shown in Table 9, a smaller value of this ratio indicates higher effectiveness of the T&E coupling. In other words, systems with a lower R ratio exhibit greater sensitivity to thermal energy, meaning that

Table 9. The value of ratio and Effectiveness of T&E coupling in different system

System	Value of R	Effectiveness of T&E
HTE	4.5%	31.8%
WWRO	31.4%	7.72%

even a small amount of thermal energy can effectively increase the system temperature, thereby enhancing overall performance under the T&E coupling strategy. This conclusion also implies that, for industrial processes with high energy sensitivity, the T&E coupling strategy can be an effective approach to enhance production, particularly when supported by an appropriate thermal energy recovery system.

5. Conclusion and Future Work

In this study, a NR-HES was proposed using Flownex, where solar and nuclear energy are coupled through the CHS to enhance electricity production. This coupling increased electricity generation by 34%. However, due to the absence of a dynamic energy control system, power production fluctuations increased by 59%. Therefore, implementing a control system in the Flownex environment might be the meaningful future work to increase control stability of the designed system. Even without such a control system, the CHS still demonstrates improved performance in mitigating the duck curve compared to a traditional PV system.

Additionally, the T&E coupling strategy is demonstrated to be an efficient approach for enhancing the production of both clean water and hydrogen. However, its effectiveness depends on the system's sensitivity to thermal energy. Systems with higher sensitivity benefit more significantly, as even a small amount of thermal energy can lead to substantial improvements. This conclusion provides useful guidance for industrial processes where thermal energy sensitivity is a critical factor.

As an initial study using Flownex to investigate NR-HES, the goal of the present study is to demonstrate that Flownex can serve as a useful tool for simulating NR-HES and potentially act as a secondary platform to support the validation of simulation results obtained from Modelica. However, due to the absence of a global control system, the proposed NR-HES cannot intelligently adjust its electricity and thermal energy output to optimize system performance and meet the demands of the local electricity grid. Addressing this limitation will be part of our future work.

In addition, Flownex provides multiple access points for integration with other commercial software, such as Ansys Fluent and NIST Fluid. By coupling with high-fidelity 2D or 3D simulations, Flownex can enable a more comprehensive analysis of NR-HES. Furthermore, the current study lacks an economic assessment, which is essential for evaluating the system's feasibility. This aspect will also be incorporated in our future research.

References

[1] International Atomic Energy Agency (IAEA), 2023, "Nuclear-Renewable Hybrid Energy Systems", IAEA Nuclear Energy Series No. NR-T-1.24, https://www.iaea.org/publications/15098/nuclear-renewable-hybrid-energy-systems.

[2] Suman, S., 2018, "Hybrid nuclear-renewable energy systems: A review", J. Clean. Prod., **181**, 166-177.

[3] El-Emam, R.S., Constantin, A., Bhattacharyya, R., Ishaq, H., and Ricotti, M.E., 2024, "Nuclear and renewables in multipurpose integrated energy systems: A critical review", Renew. Sustain. Energy Rev., **192**, 114157.

[4] Li, C.Z., Wang, L.G., Zhang, Y.Z., Yu, H.Y., Wang, Z., Li, L., Wang, N.L., Yang, Z.P., Marechal, F., and Yang, Y.P., 2023, "A multi-objective planning method for multi-energy complementary distributed energy system: Tackling thermal integration and process synergy", J. Clean. Prod., **390**, 135905.

[5] Arunachalam, M., Yoo, Y.W., Al-Ghamdi, A.S., Park, H.W., and Han, D.S., 2024, “Integrating green hydrogen production with renewable energy-powered desalination: An analysis of CAPEX implications and operational strategies”, Int. J. Hydrogen Energy, **84**, 344–355.

[6] Yu, S., Yang, Y., Chen, S.Q., Xing, H.W., Guo, Y.N., Feng, W.J., Zhang, J.C., and Zhang, J.H., 2024, “Study on the Application of a Multi-Energy Complementary Distributed Energy System Integrating Waste Heat and Surplus Electricity for Hydrogen Production”, Sustainability, **16**(5), 1811.

[7] Wang, Y.J., Yin, Y.G., Kang, Z.X., and Fan, H.T., 2025, “Thermodynamic Analysis of Pumped Thermal Energy Storage System Combined Cold, Heat, and Power Generation”, Energies, **18**(3), 525.

[8] Ji, C.X., Xie, X.Y., Chen, S.C., Cheng, M.S., and Dai, Z.M., 2025, “Optimization of a Nuclear–CSP Hybrid Energy System Through Multi-Objective Evolutionary Algorithms”, Energies, **18**(9), 2189.

[9] Harrison, T.J. and Greenwood, M.S., 2016, “Nuclear Hybrid Energy Systems Initial Integrated Case Study Development and Analysis”, Oak Ridge National Laboratory, ORNL/TM-2016/707, https://info.ornl.gov/sites/publications/files/Pub71946.pdf.

[10] Cetiner, M.S., Greenwood, M.S., Harrison, T.J., Qualls, A.L., Yigitoglu, A.G., and Fugate, D.L., 2016, “Nuclear Hybrid Energy System FY16 Modeling Efforts at ORNL”, Oak Ridge National Laboratory, ORNL/TM-2016/418, https://info.ornl.gov/sites/publications/files/Pub69372.pdf.

[11] Hills, S., Dana, S., and Wang, H.L., 2021, “Dynamic modeling and simulation of nuclear hybrid energy systems using freeze desalination and reverse osmosis for clean water production”, Energy Convers. Manag., **247**, 114724.

[12] Masotti, G.C., Cammi, A., Lorenzi, S., and Ricotti, M.E., 2023, “Modeling and simulation of nuclear hybrid energy systems architectures”, Energy Convers. Manag., **298**, 117684.

[13] Jacob, R.A., and Zhang, J., 2023, “Modeling and control of nuclear–renewable integrated energy systems: Dynamic system model for green electricity and hydrogen production”, J. Renewable Sustainable Energy, **15**, 046302, https://doi.org/10.1063/5.0139875.

[14] Flownex, Flownex Simulation Environment – Precise 1D simulation.

[15] WEC Energy Group, 2023, “WEC Clean Energy”, Retrieved 2023-01-08, Accessed 15 May 2025, https://www.wecenergygroup.com/

[16] European Commission, “Photovoltaic Geographical Information System (PVGIS)”, Accessed 10 April 2024, https://joint-research-centre.ec.europa.eu/photovoltaic-geographical-information-system-pvgis_en.

[17] World Nuclear Association, 2023, “Small Modular Reactors”, Accessed 12 August 2025, https://world-nuclear.org/.

[18] Serp, J., Allibert, M., Beneš, O., Delpech, S., Feynberg, O., Ghetta, V., Heuer, D., Holcomb, D., Ignatiev, V., and Kloosterman, J.L., *et al.*, 2014, “The molten salt reactor (MSR) in generation IV: Overview and perspectives”, Prog. Nucl. Energy, **77**, 308-319.

[19] Medrano, M., Gil, A., Martorell, I., Potau, X., and Cabeza, L.F., 2010, “State of the art on high-temperature thermal energy storage for power generation. Part 2 — Case studies”, Renew. Sustain. Energy Rev., **14**(1), 56-72.

[20] International Atomic Energy Agency (IAEA), 1986, “Design of the Reactor Coolant and Associated Systems in Nuclear Power Plants”, IAEA Safety Series No. 50-SG-D13, IAEA, Vienna, https://regelwerk.grs.de/sites/default/files/cc/dokumente/dokumente/DS481-MS_Resolutions_Trackchanges.pdf.

[21] White, F.M., 2011, “Fluid Mechanics”, 4th ed., McGraw-Hill, New York.

[22] Agata Godula-Jopek, 2015, “Hydrogen Production: by Electrolysis”, 1st ed., Wiley-VCH Verlag GmbH & Co. KGaA, Hoboken, New Jersey.

[23] Umair, S.M., Elnajjar, E., Abu-Nabah, B.A., and Hamdan, M.O., 2025, “Electrochemical and thermodynamic analysis of alkaline water electrolysis: Design and performance optimization”, Int. J. Hydrogen Energy, **128**, 643-655.

[24] Yan, X.L., and Hino, R., 2011, “Nuclear Hydrogen Production Handbook-Green Chemistry and Chemical Engineering”, CRC Press, New York, https://doi.org/10.1201/b10789.

[25] Grigoriev, S.A., Porembsky, V.I., and Fateev, V.N.,

2006, “Hydrogen production by PEM water electrolysis: research and development activities”, Int. J. Hydrogen Energy, **31**(2), 171-175.

[26] Gide, V.G., 2011, “Energy consumption and recovery in reverse osmosis”, Desalination and Water Treatment, **36**(1-3)**,** 239-260.

[27] Xylem Company, Hydranautics Seawater RO Membrane SWC5-LD, https://www.xylem.com.

[28] Ministry of the Interior and Safety, 2025, “Public Data Portal”, Accessed 16 December 2025, https://www.data.go.kr/en/index.do.